Creep properties of 9Cr and 14Cr ODS tubes tested by inner gas pressure

Denis L Sornin, Ulla Ehrnstén, Nathanaël Mozzani, Juhani Rantala, Mario Walter, Alexander Hobt, Jarir Aktaa, Elvira Oñorbe, Mercedes Hernandez-Mayoral, Andreas Ulbricht, et al.

Creep properties of 9Cr and 14Cr ODS tubes tested by inner gas pressure

D. Sornin[a*], U. Ehrnstén[b], N. Mozzani[c], J. Rantala[b], M. Walter[d], A. Hobt[e], J. Aktaa[d], E. Oñorbe[f], M. Hernandez-Mayoral[f], A. Ulbricht[g], S. Gicquel[c], L. Frank[h], Y. de Carlan[a]

[a] Université paris-Saclay, CEA, Service de Recherches Métallurgiques Appliquées,91191, Gif-Sur-Yvette, France

[b] Technical Research Centre of Finland Ltd, Vuorimiehentie 3, Fi-02044 VTT, Espoo, Finland

[c] EDF Lab Les Renardières, Mechanics and Materials of Components Departement, 77250, Ecuelles, France

[d] Institut für Angewandte Materialien, Karlsruher Institut für Technologie, KIT, Hermann-von-Helmholtz-Platz 1, 76344 Eggenstein-Leopoldshafen, Germany

[e] Materialprüfungsanstalt (MPA) Stuttgart. Actual address: FORM+TEST Seidner&Co. GmbH. Zwiefalter Str. 20. D-88499 Riedlingen

[f] CIEMAT, Division of Materials of Energy Interest. Avenida Complutense, 40; 28040-Madrid, Spain

[g] Helmholtz-Zentrum Dresden-Rossendorf (HZDR), Bautzner Landstr. 400, 01328 Dresden, Germany

[h] Materialprüfungsanstalt (MPA) Universität Stuttgart, Pfaffenwaldring 32, 70569 Stuttgart, Germany

* Corresponding author: denis.sornin@cea.fr

Author Name	ORCID	Email address
Denis L. Sornin	https://orcid.org/0000-0002-9745-0299	denis.sornin@cea.fr
Ulla Ehrnstén	https://orcid.org/0000-0002-3573-1749	Ulla.Ehrnsten@vtt.fi
Nathanaël Mozzani	https://orcid.org/0000-0003-2739-6415	nathanael.mozzani@edf.fr
Juhani Rantala	https://orcid.org/0000-0001-8170-4365	Juhani.Rantala@vtt.fi
Mario Walter		mario.walter@kit.edu
Alexander Hobt	https://orcid.org/0000-0002-6022-8459	hobt@formtest.de
Jarir Aktaa		Jarir.aktaa@kit.edu
Elvira Oñorbe	https://orcid.org/0000-0002-6080-2844	Elvira.Onorbe@ciemat.es
Mercedes Hernandez-Mayoral	https://orcid.org/0000-0003-4504-7577	m.mayoral@ciemat.es
Andreas Ulbricht		a.ulbricht@hzdr.de
Solene Gicquel-Petit	https://orcid.org/0000-0002-1200-8988	solene.gicquel@edf.fr
Lukas Frank	https://orcid.org/0000-0002-4906-0173	Lukas.Frank@mpa.uni-stuttgart.de
Yann de Carlan	https://orcid.org/0000-0001-8522-9004	yann.decarlan@cea.fr

Highlights:

- 9Cr and 14Cr ODS steel tubes are creep tested by inner gas pressure representative of the fission gas loading encountered in service conditions.
- Creeps tests handled by 4 different European teams with different experimental set-up are consistent showing a very low scattering
- The ODS steel tubes typical failure mode is leakage without burst on a longitudinal crack occurring at very low hoop strain.

Key words: ODS steel, Tube creep test, Inner gas pressure

Abstract:

Oxide-dispersion strengthened steels are promising materials for extreme service conditions including nuclear reactors core. In service conditions, nuclear fuel claddings are exposed to the fission gas pressure at temperatures about 700°C. This paper presents novel results on ODS creep properties from a round robin of inner gas pressure creep test. A gas pressure creep test, simulating fission gas loading, was designed and achieved by four different European teams. Lifetime and specific behavior of ODS steel tube are prospected. Based on a mechanical clamping achieving gas tightness, short length tubes samples are tested by different laboratories. In-situ laser measurements exhibits the radial expansion of ODS steel tubes before failure. Post mortem, geometrical characterizations are performed to determine hoop strains at failure. A consistent creep lifetime is observed by all the teams even with slightly different testing apparatus and clamping systems. Under inner gas pressure, ODS steels exhibits a typical failure by leakage associated to a very small radial expansion. This behavior results from a brutal failure (burst) without evidence of tertiary creep stage. This failure mode of ODS cladding in creep conditions is consistently observed on all samples of the study. Inner gas pressure creep tests where compared, for the first time, by four European laboratories on ODS steel tube. This technique, simulating the fission gas pressure loading, is applied on small and mechanically clamped samples. This technique shows a remarkable consistency between the different laboratories results and demonstrates to be efficient for ODS steel cladding tube qualification. The results show a correlation between the creep properties and the microstructure.

1. Introduction

Considering technical and economic issues, the coming generation of Sodium Fast nuclear Reactors (SFR) must achieve very high fuel burn-ups. Therefore, the choice of materials is crucial to guarantee safety and reliability of the core components. Most of the structural components of the core are made of stainless steel to provide corrosion resistance in both service and fuel reprocessing conditions [1, 2]. As to prevent geometrical distortion at high burn-up, the ferritic grades exhibiting a very low void swelling under irradiation are, however, preferred [3-5]. Within this framework, ODS ferritic steels are foreseen for the fuel cladding material [6-8]. The very fine and stable nanoprecipitation of oxides hinders the dislocation mobility at high temperature which results in the good creep properties of the ODS steels [9], [10]. In service conditions, the tubes must withstand the fission gases pressure at high temperature (about 700°C). At the same time the cladding material is submitted to a neutron irradiation up to 150 dpa. The assessment of creep properties was first made using tensile samples made from bars or a massive block [11, 12]. However, the ODS steel microstructures are known to be very anisotropic, which depends on the used manufacturing and forming processes [13]. Thus, creep results are very dependent on both the microstructure and testing direction [14],[15].

Since 2012, CEA manufactures cladding tubes from Hot Extruded rough bars [16], further cold formed by tube pilgering [17]. To assess the behavior of such cladding tubes with a complex microstructure inherited from the manufacturing sequence, the need of advanced creep test emerge. Such tests are expected to be demonstrative of the real loading path during service [18]. However, to perform creep tests on tubular materials, the tube specimen must be plugged to retain the pressure inside the tube, which is not a trivial challenge. Therefore, within the framework of the European EU-MatISSE project, a task was dedicated to inner pressure creep tests on ODS cladding tubes involving four Europeans teams which developed their own plugging system and test apparatus and performed the tests.

Welding is the most typical technique used for plugging conventional materials for internal pressure creep tests. However, ODS-materials lose their creep strength when melted, which must be taken into account when designing the test set-up. Rather little openly available information on ODS tube material internal pressure tests and plugging techniques was found in literature [18], [15]. Different methods for plugging have been prospected in earlier study [19]. Pressurized resistance welding (PRW) was often selected over uniaxial diffusion welding, spark plasma sintering or friction stir welding [18] [20]. Magnetic pulse welding [21] and friction stir welding [22] have also been developed for welding fuel bundle plugs.
For example, JAEA has developed tubes creep tests using two end plugs welded by PRW [18]. This technics enables a large number of tests in the same furnace [23], [24] but is not optimal considering the deformation monitoring during testing. At CEA, electron beam welding is used for manufacturing of long samples where welded regions are protected during testing by water boxes [15]. This last technique is expensive and material consuming due to the complexity of the sample apparatus.

In the present work, a mechanical plug was developed and used. A mechanical plug allows more efficient use of the material, as the HAZ of the welds does not need to be protected during the test, reducing the overall tube length. Moreover, for a better understanding of the failure mode of ODS tubes, diametrical expansion monitoring during testing is useful and possible. , VTT has successfully developed a mechanical plug for internal pressure testing of 15/15Ti steel tubing, which indicated that this type of plugging can also be used for ODS tubes [25]. The plugging was slightly modified for ODS materials. While KIT and MPA Stuttgart used slightly modified types of VTT's plugging system, EDF developed their own experimental system based on mechanical plugs.
In this study not only lifetime but also creep deformation were captured showing the singular failure mode of ODS steels. Post–mortem analysis were also carried out to identify the crack geometry.
This study evidence the creep behavior of ODS tubes under temperatures and loading path similar to the service conditions.

2. Materials and methods

2.1 Material manufacturing

ODS steels are the results of a complex manufacturing sequence involving powder metallurgy. Pre-alloyed gas-atomized metallic powder is used with a D50 of about 80 µm in two different Cr contents, 9 and 14 wt%. These powders are then mechanically alloyed, under H_2 atmosphere, with 0.25 wt% of Y_2O_3 and 0.3 wt% TiH_2. The nominal composition of the various grades of the study is presented in Table 1. The powders are processed in one or two Hot Extrusion batches. The powder is put in soft steel cans of about 3 kg and air vacuumed during 4 h at 400°C. After sealing, the billets are heated for 1 h at 1100°C in a radiative furnace. During this treatment, nano-oxides precipitate [26],[27]. Then the billets are Hot Extruded (HE) using a circular die and a 675 ton hydraulic press with an extrusion ratio of R=12.5. After removing the cans and deep drilling, seamless rough tubes are obtained with a diameter about ø16 mm. Before cold pilgering, a specific heat treatment is applied depending on the composition of the tubes. For the ferritic grades (14Cr), a 3 h heat treatment at 1200°C releases stress induced by hot extrusion. For the ferritic-martensitic grade (9Cr), a softer initial treatment of 1h at 1050°C is imposed. Then, a sequence of four cold working passes by High Precision Tube Rolling (HPTR) pilger mill is applied with intermediate heat treatment at 1200°C and 1050°C for 14Cr and Cr respectively. The cumulated logarithmic strain is about 40% for each of the 4 passes. The final dimensions are ø10.73x0.5 mm and a final heat treatment is applied depending on the grade. For 14Cr ODS grade, a 750°C/1 h recovery treatment is applied after the last pass whereas for the 9Cr ODS grade, quenching is applied resulting in a martensitic structure tempered at 750°C/30 min. Then, tubes are straightened and optically controlled. About 2000 mm of each grade was produced and dispatched to the EU-MatISSE project partners.

Table 1. Nominal composition of the ODS steel grades.

Grade	Nominal composition (wt-%)							Final heat treatment
	Cr	W	C	Y_2O_3	Ti	Ni	Fe	
9Cr ODS	9	1	0.1	0.25	0.2	0.15	Bal.	Quenched + tempered 760°C/30min
14Cr ODS	14	1	0	0.25	0.3	0	Bal.	750°C/1h

2.2 Microstructural investigations

SEM EBSD orientation maps are presented in Figure 1 and Figure 3 for the 14Cr and 9Cr ODS tubes, respectively. The inverse pole figures colour code is plotted respectively to the longitudinal direction (RD). ND corresponds to the radial direction of the tube. For both tubes, poles figures corresponding to the {100}, {111} and {110} planes are plotted in Figure 2 and Figure 4.

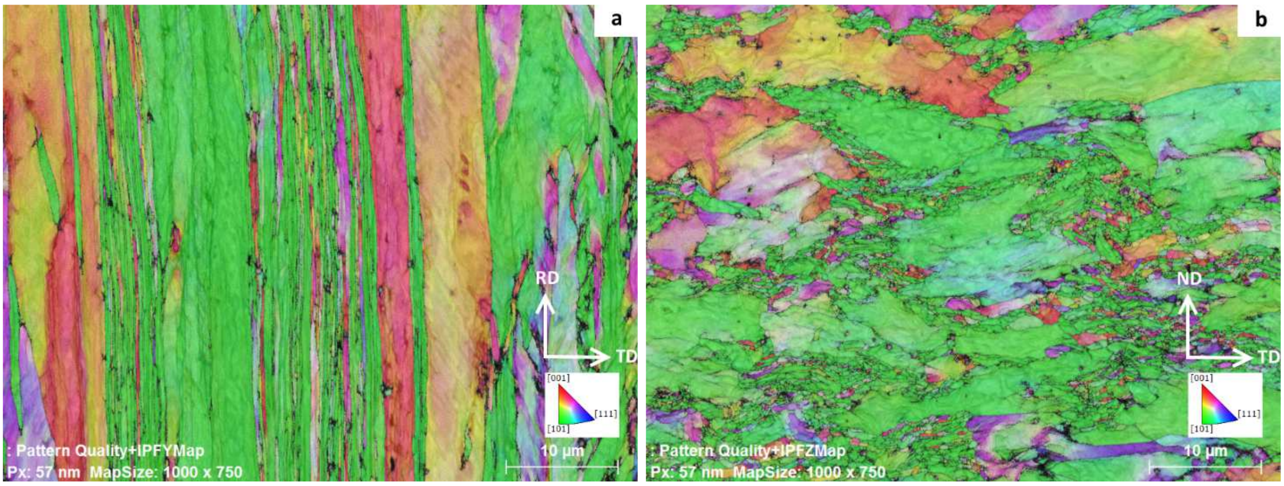

Figure 1. SEM EBSD orientation maps along RD for the 14Cr ODS tube, (a) in longitudinal and (b) transversal direction (CEA).

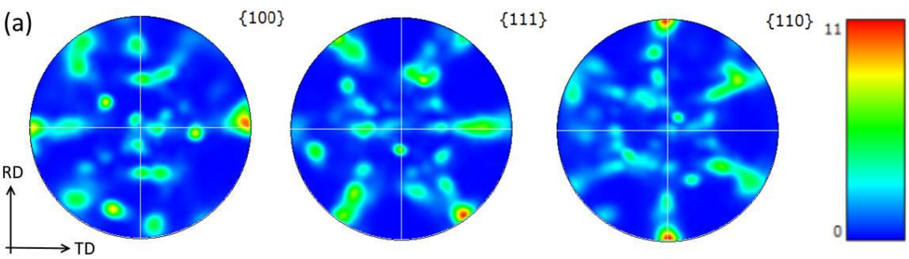

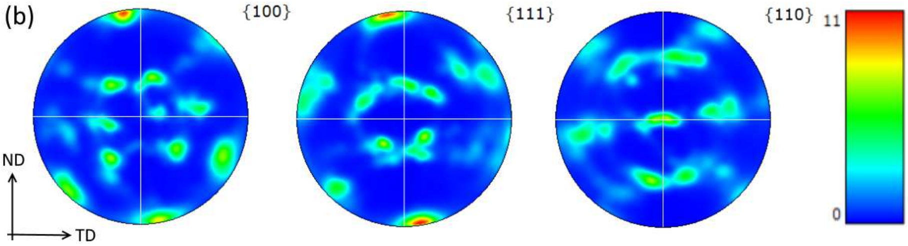

Figure 2. {100}, {111} and {110} poles figures computed from EBSD maps for the 14Cr ODS tubes projected on, (a) RD-TD and (b) ND-TD planes (CEA).

For the fully ferritic 14Cr ODS tube material, Figure 1 show clearly an anisotropic microstructure. The ferritic grains are elongated in the axial orientation with a size of tens of micrometres, while the size in the opposite direction is a few micrometres. Due to the reduced number of grain captured by the map, Figure 2 is more indicative than quantitative. However, the well-known rolling texture, α <110> fiber along rolling direction is observed for the ferritic 14Cr ODS tube. Consequently, 14Cr ODS material is assumed to exhibit strong creep properties anisotropy.

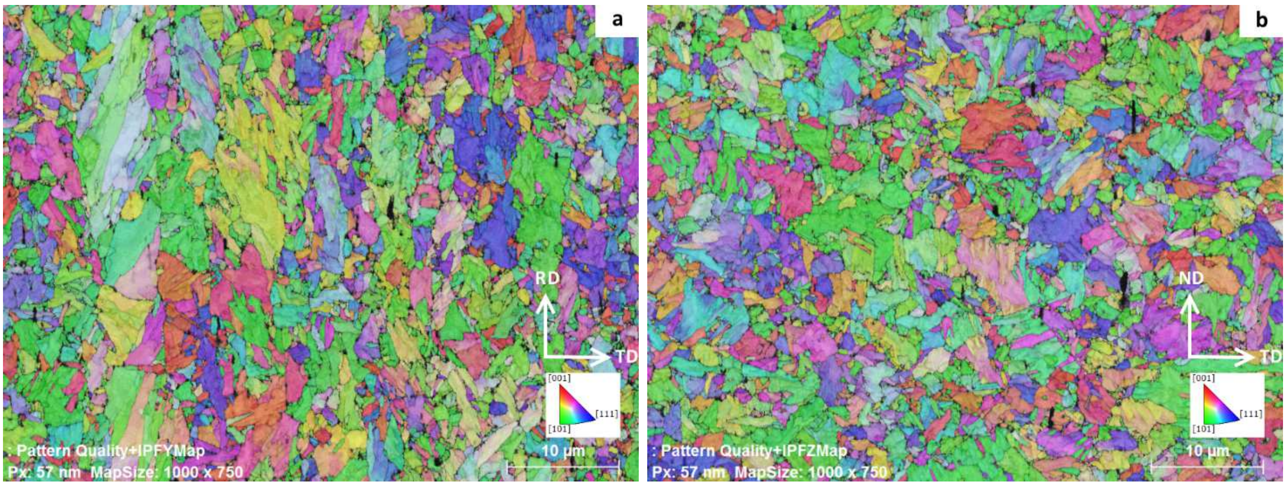

Figure 3. SEM EBSD orientation maps along RD for the 9Cr ODS (K30-M3) tube, (a) in longitudinal and (b) transversal direction (CEA).

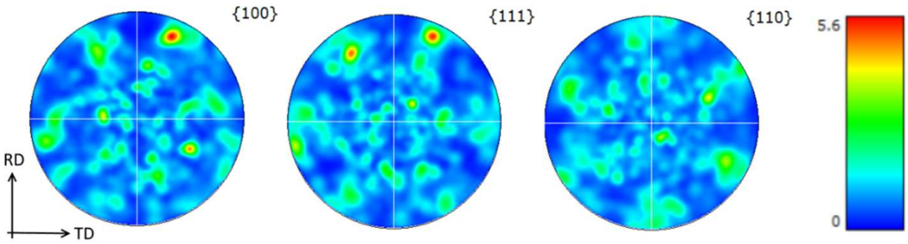

Figure 4. {100}, {111} and {110} poles figures computed from EBSD maps for the 9Cr ODS tubes projected on RD-TD plan (CEA).

The microstructure of the tempered martensite 9Cr ODS tube material is predominately constituted of equiaxed packets of few microns in size. The martensitic structure is very specific to ODS grades with less than 11 wt% Cr. It comes from previous austenitic grains that are only a few microns in size. This leads to a transformation in which one variant per previous martensitic grain is often observed. To the end, at the macroscopic scale, a rather isotropic structure is obtained. It is formed of small packets of ferrite laths, very entangled, which are difficult to discern by SEM.

A weak α fiber is noticed in Figure 4 compared to 14Cr ODS. Contrary to the Japanese 11Cr ODS grade [28], the material is entirely constituted of martensitic domains excluding residual ferrite.

Specimens for TEM observations were prepared by electrolytic polishing of 3 mm discs drilled from the tube wall, using the reactive mixture of 5% perchloric acid and methanol at -60 ºC. Usual imaging methods such as Bright Field (BF) and Weak Beam Dark Field (WBDF) were employed in a TEM JEOL JEM-2010 with LaB_6 filament operated at 200 keV. Size distribution was estimated by image analysis technique measuring the longer axis of precipitates, using at least five different areas for each measurement employing JMicroVision software [29]. The microstructure of the 9Cr ODS tube is also described with SEM by E. Oñorbe et al., .The same grain structure with large precipitates (mainly TiO_2 about 100 nm in dimeter) within grains and at grain boundaries was also visible [30]. Dense networks of dislocations were present within grains and a homogeneous distribution of nano-oxides where dislocations were pinned. The microstructure of 14Cr ODS tube consisted in large columnar ferritic grains with a high dislocation density after rolling process. Figure 5 shows an example of the fine distribution of nano-oxides in the 14Cr ODS. Figure 6 shows the size distribution obtained for both materials. Precipitates appear smaller in 14Cr ODS grade compared to the 9Cr martensitic ODS steel with an average diameter (2.4±0.9) nm in 14Cr and (4±1) nm in 9Cr ODS.

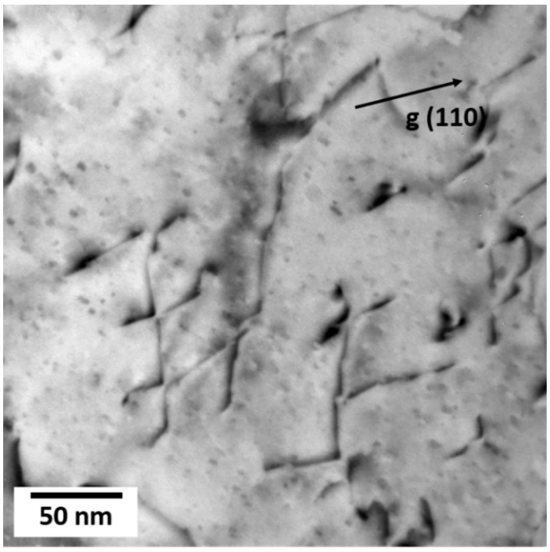

Figure 5. TEM BF image of the dispersion of nano-oxides in 14Cr ODS tube (CIEMAT).

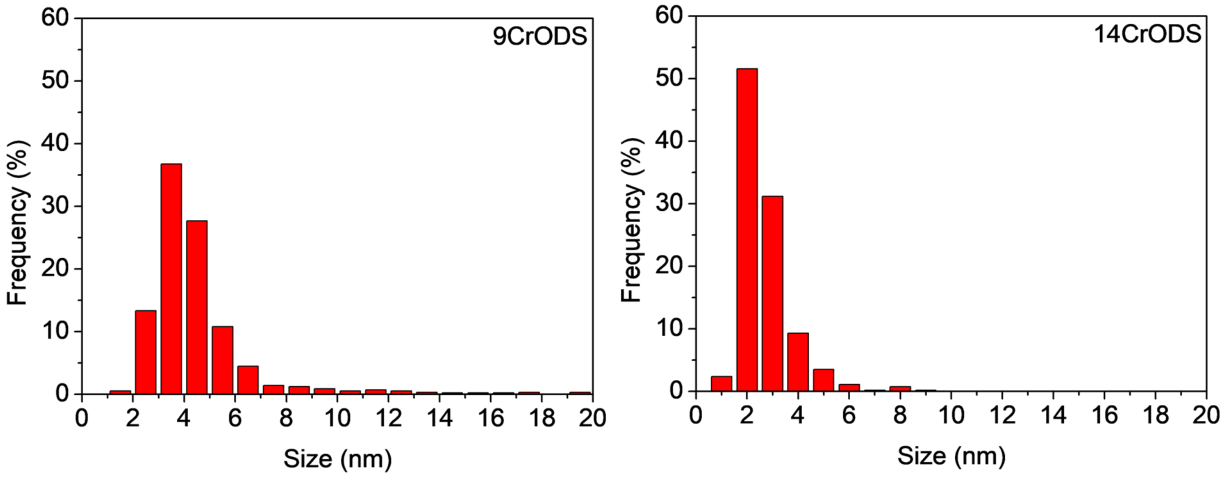

Figure 6: Size distribution (diameter) of nano-oxides as measured by TEM in 9Cr ODS and 14Cr ODS tubes (CIEMAT).

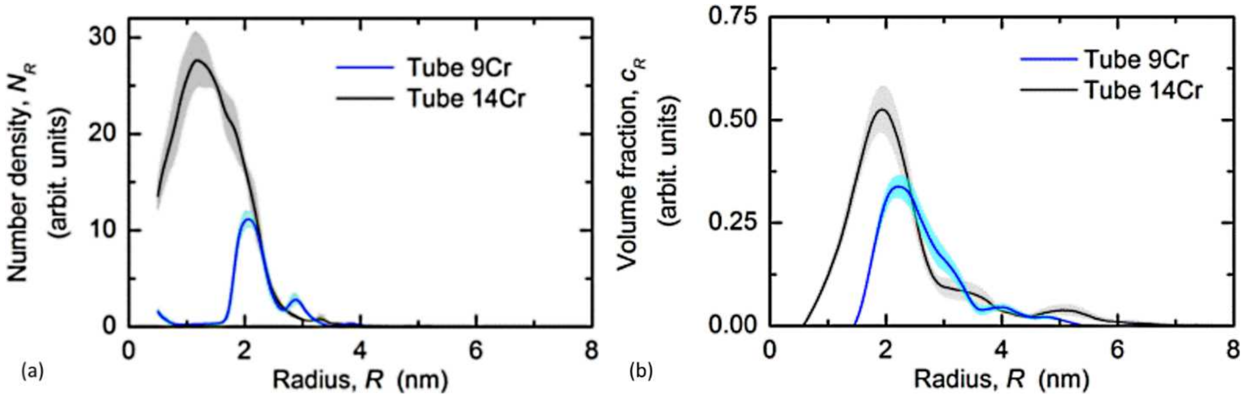

Figure 7. SANS characterization, (a) size distributions in terms of number density of scatters per size increment, (b) size distributions in terms of volume fraction of scatters per size increment (HZDR).

Precipitate distribution was also determined using Small Angle Neutron Scattering (SANS) for both 14Cr and 9Cr ODS grades on D22 at ILL Grenoble [31]. In Figure 7, the maximum density is noticed at 1.5 nm for 14Cr ODS and about 2 nm for 9Cr ODS. Density appears slightly higher in 14Cr compared to 9Cr ODS. Both SANS and TEM characterizations consistently exhibit a fine precipitation in both materials with a higher density and reduced size in 14Cr compared to 9Cr ODS.

2.3 Creep testing

Internal pressure creep tests were performed by four laboratories using tube specimens with 45 mm length (one laboratory used 90 mm long specimens). A short specimen length was mainly chosen based on the amount of tube length available for the tests. Before the tests were started, the plugging of the tubes using mechanical plugging had to be developed and verified. All laboratories were successful in this task. The internal pressure tests were performed at 700°C and pressures between 90 and 120 bar for the 9Cr ODS tube material, and at both 650° and 700°C and pressures between 100 and 181 bar for the 14Cr ODS tube material

2.3.1 Creep testing at VTT

The principle of the mechanical plugging at VTT is based on two conical clamping rings compressed against each other as shown in Figure 8. The Multi Physics software was used in the selection of plug material and plug structure. Stress analyses were performed using Iron Cad software with a Multi physics program. According to these calculations, the best materials for both the plug beads and rings is 304 stainless steel. Compressive stresses were confirmed at the plug, and the structure did not cause any stress localisation in the tube close to the plug.

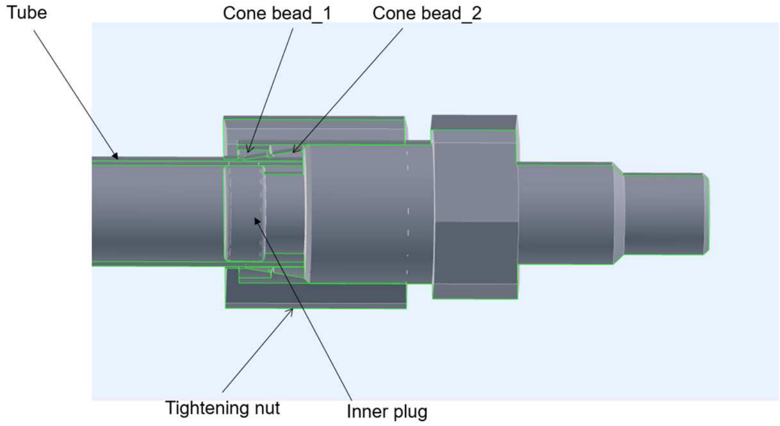

Figure 8. Drawing showing the plugging design by VTT.

Two thermocouples were installed in the middle of the specimen gauge section, but not tied onto to the tube to avoid scratching. ODS-materials are known to be very notch sensitive, and scratches could easily affect the results. The tube specimens were pressured using argon gas, while the environment on the outer surface was air. The tests were mainly continued until failure. In a few cases, the tests were interrupted without failure after 1800 hours. The last test was performed using biaxial loading with axial/hoop stress ratio of 1. The main intention of this was to demonstrate the effectiveness of the plugging in this type of loading for future use. Biaxial testing is useful to produce data for improved models incorporating the material anisotropy, but also to produce data for different loading scenarios during use, including dry storage, where biaxial loading may prevail. The location of the crack was determined after the test to evaluate a possible influence of the plugging on the results. Most specimens were also subjected to dimensional measurements and scanning electron microscopy (SEM).

2.3.2 Creep testing at EDF

The experimental setup, used by EDF for the ODS cladding tubes, was originally designed for testing Zirconium alloy claddings for pressurized water reactors (PWR). Argon is used as the pressurizing gas. The furnace was modified at the beginning of the EU-MatISSE project in order to reach higher temperatures (up to 800°C) and to accommodate to tube burst (i.e., adding an inner shield to the furnace). Several creep-to-rupture tests were performed on Zircaloy cladding and were successful. Temperature homogeneity was checked at 800°C, and an 8°C gradient was found on 120 mm long specimens. Maximum temperature was measured at the middle of the specimen and the lowest near the bottom plug. Such temperature variations will ensure that failure will occur near the middle of the specimen, as was effectively seen in the tests.

During the test, the cladding deformation is monitored at mid-length by a laser with an accuracy of 5 µm (<0.1 %). The maximum pressure available is 500 bar. Three thermocouples are taped to the specimen to control the furnace. Before and after testing, dimensional controls are performed on the specimen. Based on the experience achieved from PWR cladding tube testing, the chosen plugging technique is inspired by the Swagelok tube fitting principle, but several improvements were undertaken for ODS cladding tubes. The use of an inner filling part on which the tube will collapse was introduced and the different materials were changed to take into account the high mechanical strength of ODS tubes and the need to reuse the pressure fittings. Since the available tube-length is small, only 90 mm long specimens were used, instead of 120 mm for Zircaloy tubes. The first high temperature tests were performed using another ODS test tube provided by CEA. These proved the homogeneity of temperature (±1 % along the specimen) and the tightness of the circuit.

2.3.3 Creep testing at KIT

At KIT, a universal INSTRON (Type 4505) testing machine, equipped with a 5-zone radiation furnace, was used. To apply a controlled internal pressure using argon during testing, a new pressure unit was built, allowing pressurizing a sample between 10 and 200 bar with a deviation of less than 0.3 bar related to a set value. After completion, the entire test facility was successfully validated by different specified tests on welded Zircaloy 4 specimens. Additionally, one test on an ODS test tube sample was performed in order to ensure the usability of slightly modified mechanical clamps, originally developed at VTT.

For post-test investigations, a customized laser measurement device from ANT Antriebstechnik GmbH (Germany) with a measurement accuracy of 1 µm was used to generate 3D scans of the tested samples to determine the shape evolution depending on the test conditions. The measurements were conducted such, that the diameter of a sample was determined over the entire length for a multitude of positions, using a step size of 500 µm between two adjacent positions. In order to examine the roundness of a specimen, a sample was rotated degree-wise at every longitudinal position and 360 values per plane were measured (generally, it would be enough to measure up to a rotation of 180° since afterwards the measurement is more or less repeated). Afterwards, the diameter at every longitudinal position was calculated by averaging the 360 measured values and finally, these averaged values were used to calculate the related hoop strains at the outer surface along a sample.

2.3.4 Creep testing at MPA

At MPA Stuttgart, a plugging type, modified based on the VTT design, was applied. The tube was clamped between conical elements, allowing a minimum influence on the notch sensitive material. The specimen was tested in a 4 column servo-hydraulic universal test machine with a new control electronics. The specimen was heated using a 3-zone radiation furnace. Three thermocouples were applied to measure the temperature along the load train: one couple on each specimen grip and one on the centre of the specimen. The temperature gradient could be kept below 1°C and is in accordance to the given requirements for standard creep tests. The pressure was applied with compressed argon gas. During the creep tests, axial load was zero. This means that only the effect of the inner pressure is accommodated within the tube itself. The pressure was applied after heating up of the system and kept constant within 2% of accuracy. The pressure inlet had a certain length inside the heated area to avoid re-cooling of the tube when applied the pressure and gas flow into the tube. The axial strain was measured during the test using a high temperature contacting extensometer. The contact pressure of the extensometer was minimised since the final failure crack was at a different position than the contact points. The length and the diameter were measured both before and after the test with a precise light projector which is capable of measuring small dimensions. It is commonly used at the MPA to measure creep strain.

3. Results

3.1 Creep properties

The results from the internal pressure tests are presented in Figure 9. The behavior of the tube materials is very consistent, with smaller scatter than what is usually observed in this type of results even for conventional industrial materials.

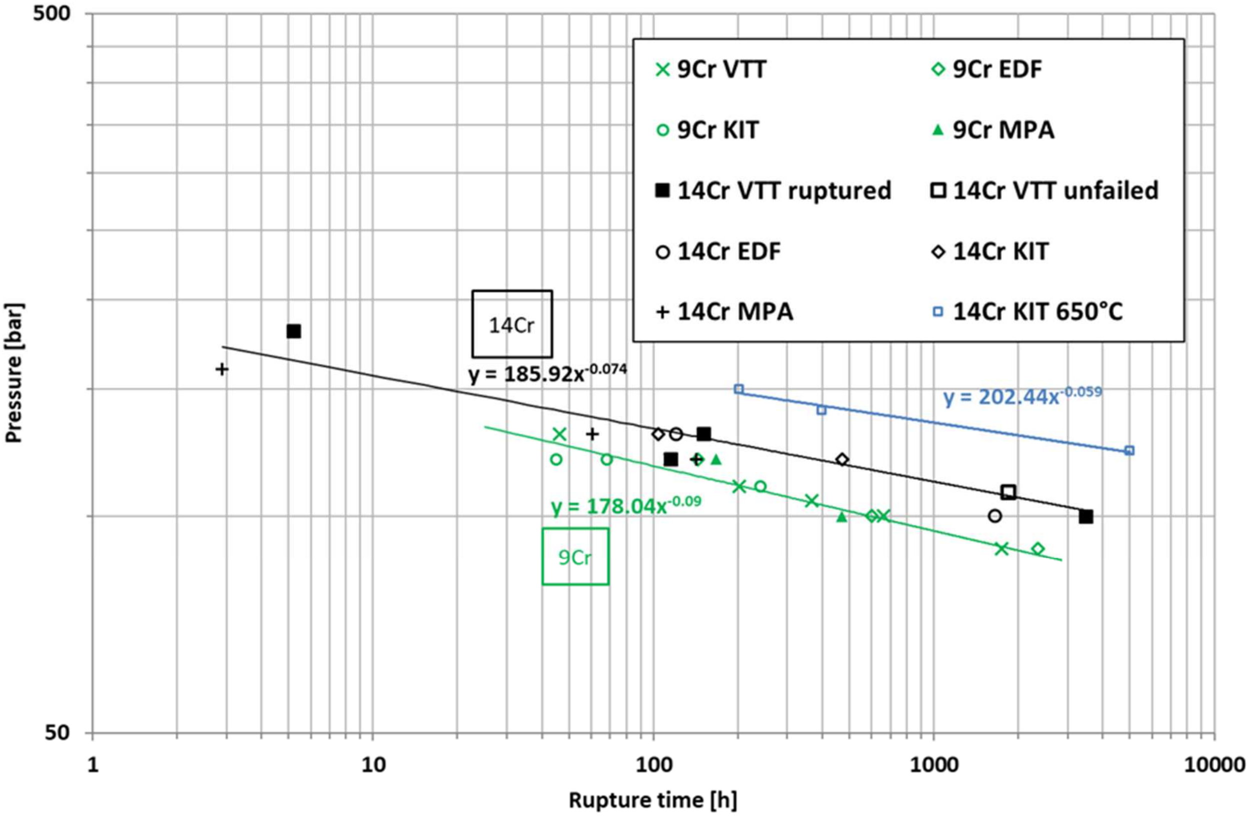

Figure 9. Monkman-Grant plot of Internal pressure creep test at 700°C. Pressure as function of lifetime for 9Cr and 14Cr ODS tubes.

The creep stress results are plotted as a function of the Larson-Miller parameter (with constant C=30) in Figure 10. By modifying the C-parameter of the LMP parameter, it was possible to fit the results of each material on a single line. The Mean Diameter Hoop stress is defined by equation 1, where *p* is the gas pressure, *D* is the external tube diameter and *t* the tube thickness.

$$\text{MDH Stress} = p\,\frac{(D-t)}{2t} \qquad Eq. 1$$

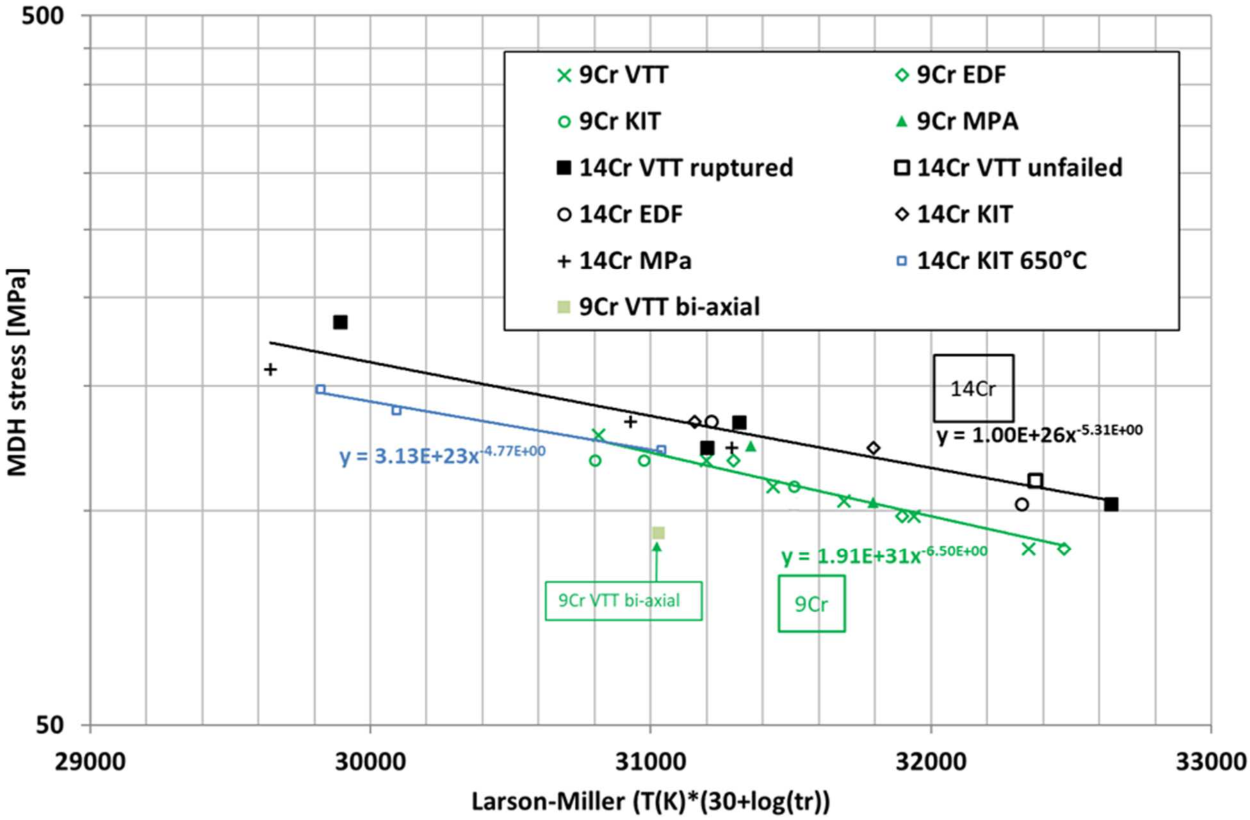

Figure 10. Internal pressure tube creep test results at 700°C. Mean diameter hoop (MDH) stress as function of the Larson-Miller parameter.

The 14Cr ODS tube is clearly superior to the 9Cr ODS tube in terms of lifetime. This behavior could be explained by the significant difference in nano-precipitation density between the two grades. The biaxial test using 9Cr ODS tube was successful and showed a shorter lifetime than those obtained using internal pressure only. With only one biaxial test result further conclusions on possible reasons for the shorter lifetime will not be done. The exact test conditions are summarized in the supplementary tables S1 and S2 for 14Cr ODS and 9Cr ODS tubes, respectively (Please refer to electronic supplementary material).

The on-line diametric measurements, i.e., the creep curves, performed by EDF, are shown in Figure 11. The creep hoop strains at failure are small in both materials, but smaller in the 14Cr ODS tube material compared to the 9Cr ODS tube material.

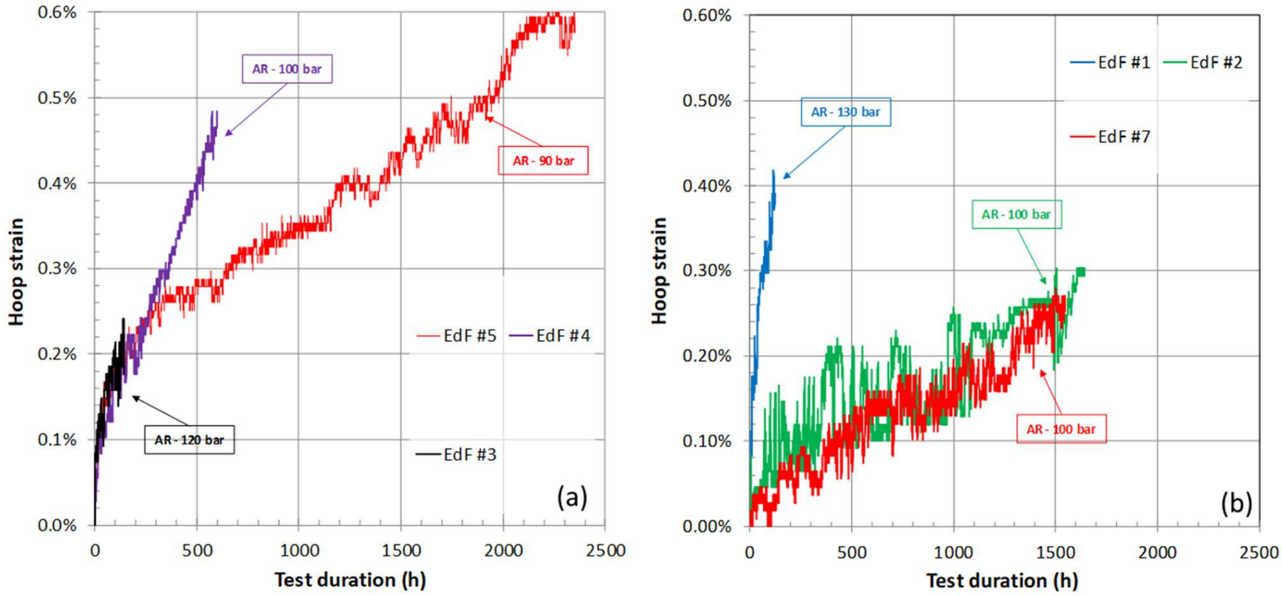

Figure 11. Creep curves for (a) 9Cr and (b) 14Cr ODS tube specimens (EDF).

It is clear that leakage and final failure of tube occurs without any tertiary creep stage. Minimal creep strain rate is lower for the 14 Cr ODS material compared to 9Cr ODS material at all stress levels. Even for the 9Cr ODS material, the overall hoop strain does not exceed 1 %. Considering the fuel cladding-tube application, this failure mode without burst is beneficial because it minimizes the impact of a possible burst on the coolant flow around the tube. At the same time, the very narrow crack helps in retaining the solid fuel pellets inside the tube.

3.2 Results from post-test analysis

The length of the cracks after failure were typically a few mm, and they locate at least a few mm away from the plug (Figure 12 and Figure 13), strongly implying that the test results were not influenced by the plugs. Typically, the specimens contained one main crack after rupture, parallel to the rolling direction, with secondary smaller cracks near the main one. This was observed in both materials, although this feature was stronger in the 14Cr ODS material, Figure 12 (b). This behavior relates probably to the columnar microstructure of the cold rolled tubes. Previous creep studies, driven on massive samples machined perpendicular to the extrusion direction have shown a preferential crack propagation along the grain boundaries [12]. Thus, the cracks are probably prone to propagate along the grain boundaries in tubes also. The fracture surfaces were heavily oxidised, and the cracks morphology could not be determined. The oxidation is obviously occurring during the creep test. At VTT, the furnace cooling down after failure can take a few hours exposing the open crack surface to high temperature air and thus oxidation.

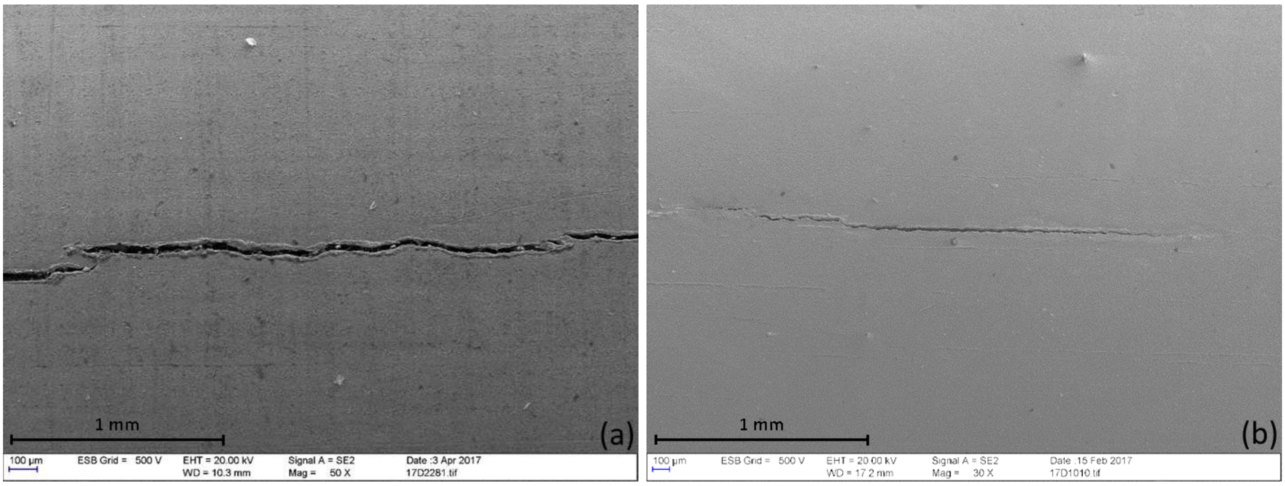

Figure 12. SEM pictures of (a) 14Cr ODS tube specimen after failure (tested at 700 ℃ - 120 bar), (b) 9Cr ODS tube creep specimen after failure (tested at 700°C - 90 bar) . Several separate short cracks are seen near the main crack, causing the leak (VTT).

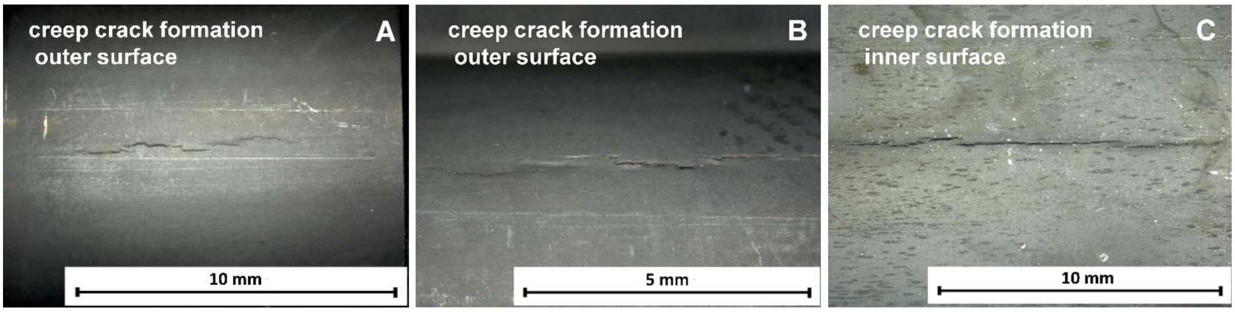

Figure 13. Optical microscope pictures of a 14Cr ODS tube (tested at 700°C - 130 bar) - creep crack formation: (A), (B) outer surface, (C) inner surface (KIT).

The main crack has almost the same length on the inner and outer sides of the tube, Figure 13, and the leak is assumed to be due to this single narrow crack.

Based on diametric measurements after the test, the failure strains were in all laboratories found to be smaller than 1% (mostly about 0.6 %). Figure 14 presents the measured strains in a 14Cr ODS tube, along various lines and angles. Some localisation of deformation was observed, indicating that the local failure strain is higher than the overall failure strain, and can be up to four times higher.

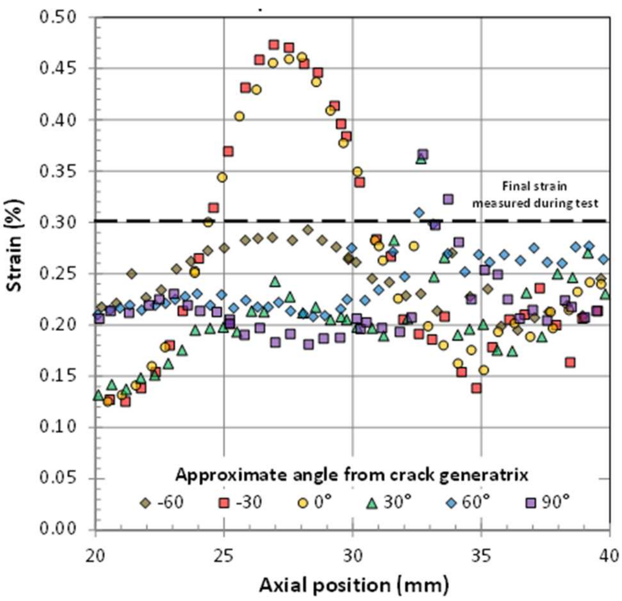

Figure 14. Post-test dimensional measurement for a 14Cr ODS tube specimen (tested at 700 ℃-100 bar) (EDF).

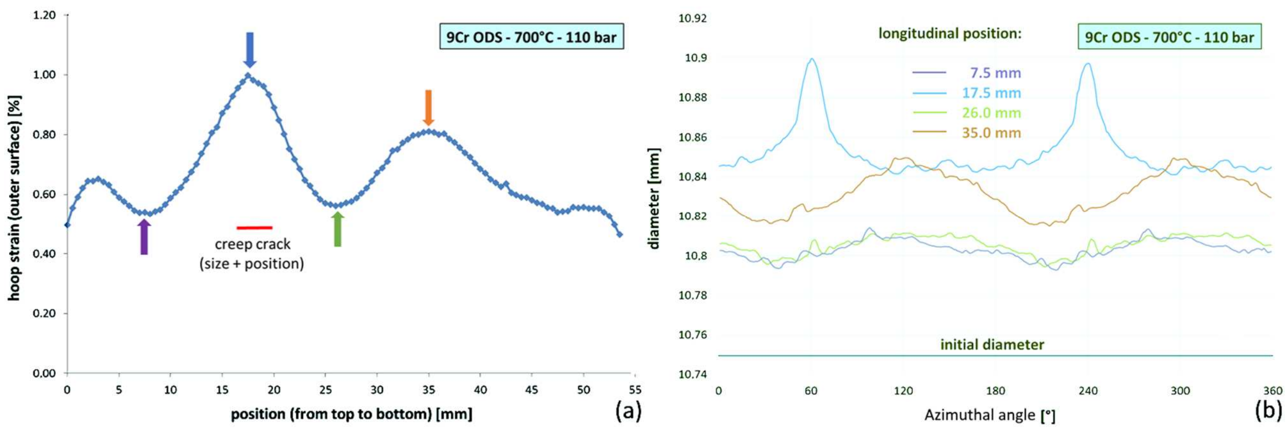

Figure 15. 9Cr ODS tube creep deformations after test (tested at 700°C - 110 bar), (a) hoop strain along the tube axis and (b) Diameter along the azimuthal angle for various sections along the tube axis (KIT).

Figure 15 (a) presents the hoop deformation of a 9Cr ODS tube as a function of the axial position along the tube axis. For this figure, the hoop strain is computed as the mean values of the various generatrix. The diameter of the creep-tested sample is plotted as a function of various generatrix angles for different positions along the axis in Figure 15 (b). The axial position 17.5 mm, corresponding to the maximum hoop strain, exhibits two cracks localization peaks. For 9Cr ODS tubes, the average hoop strain at failure is approximately two times higher compared to the one in the 14Cr ODS material. Comparison of diameter, along the crack generatrix, exhibits a more uniform creep deformation for the 9Cr ODS tube compared to the 14Cr ODS one. The 9Cr and 14Cr ODS materials respective behaviors are consistent with the noticed variation of the nano-oxides population and therefore the Zener pinning force on dislocations [32]. Indeed, the 9Cr ODS material exhibits a more ductile behavior compared to the 14Cr ODS material.

4. Discussion

Microstructural analysis of both 9Cr and 14Cr ODS tubes show that grain morphology is different in the two materials. The crystallographic texture is similar but more pronounced for 14Cr compared to 9Cr ODS tube material. Nano-precipitate analysis both by SANS and TEM reveals finer precipitates and higher density for the 14Cr ODS material. This has already been documented for other ODS materials [33] and mainly attributed to the occurrence of a phase transformation at high temperature in 9Cr ODS tube material.

Creep strength of the 14Cr ODS tube material is better than that of the 9Cr ODS tube material. This is consistent with the observed differences in the nano-precipitates density that could explain a lower creep strain rate in 14Cr. It can be noticed that despite a strong microstructural anisotropy in the 14Cr ODS tube material, this is a good candidate for cladding tube application.

Previous study performs creep tests on hot extruded 14Cr ODS steel bars tested in two directions [12]. Samples in the extrusion direction are obviously stronger than the ones in the transvers direction in term of lifetime. Due to the dominant contribution of the hoop stress in gas pressure tests, the tubes strength should be compared to the transvers direction [15]. However, the tube strengths are significantly lower compared to those of the extruded bars [12]. This could be explained by the nanoprecipitation coarsening induced by the intermediate high temperature heat treatments of the pilgering sequence. At the same time, the material is constantly deformed along the axial direction increasing the microstructural anisotropy finally observed on tubes

Post-test analysis of various samples shows that cracks are relatively short and propagate exclusively in the longitudinal direction in both grades. This is consistent with the applied stress and the microstructural anisotropy issued from cold forming. For all performed tests, leakage is due to one single macroscopic crack sometime surrounded by secondary cracks in the same region. The tube leakage occurs with very small radial deformation (less than 1 %) around the main crack. Monitoring of tube samples geometry during creep shows that leakage occurs without evidence of tertiary creep stage. This behavior is consistent with documented creep tests on forged bars [10].

The tests matrix analysis shows good consistency between all results, in which partners applied various testing procedures, showing that the materials are homogenous, and are not affected by lab-to-lab variations. The creep performance of ODS tubes strongly depends on the microstructure of the material and the amount of strengthening nano-oxides. For example, with regard to martensitic ODS steels, JAEA has developed tubes with a specific ferrito-martensitic microstructure with internal pressure properties which are superior to those of the 9Cr ODS tubes tested in this study [24, 34]. Likewise, a 12Cr ferritic grade ODS with a higher W content (2wt%) than the 14Cr ODS grade studied here, exhibits lifetime significantly higher than the one observed in this project [23], [24].

Thus, depending on the technical specification imposed by the reactor design, it appears possible to increase significantly the performance of the ODS cladding tubes under internal pressure. The appropriate choice of chemical composition and manufacturing route for ODS tubes will be governed by the compromises between the various requirements of the intended application.

5. Conclusions

Ferritic ODS tubes were manufactured as thin cladding tubes and further tested in creep conditions by inner gas pressure. The creep behavior was determined for two ODS materials with different chromium content, i.e., 9Cr and 14Cr. These two materials exhibits some difference in terms of grain size and shape as well as in texture and nano-precipitate distribution. The creep test matrix using internal pressure was built in collaboration between EDF, VTT, KIT and MPA. The test set-ups differs mainly in the experimental device and tube clamping system. The following main results are obtained:

- Internal pressure creep test results obtained at 650°C and 700°C at VTT, EDF, KIT, and MPA are consistent. The same tendency are observed both for 14Cr and 9Cr ODS tube materials. All results, produced by different project partners are consistently aligned on a single Larson-miller graph despite the use of various clamping system and testing device. Thus, no lab-to-lab variation exist, and the materials are homogenous. The 14Cr ODS steel exhibits a better creep strength compared to the 9Cr ODS material. This tendency, largely documented for tensile samples from forged materials, is confirmed here for cold formed tubular materials.
- The microstructure of 9Cr and 14Cr ODS tube materials differs strongly in terms of grain size, aspect ratio and crystallographic texture. Unexpectedly, the strong microstructural anisotropy of 14Cr ferritic grade is not detrimental for the tube creep behavior.
- The observed differences between the 9Cr and 14Cr ODS tube creep strength ccan be linked to the differences in the nano-precipitate density and size.
- The samples develop a single main crack of about 10 mm long that cause leakage and stop of the test. This crack induces small hoop strain near the crack, which is limited to a few percent. Secondary cracks are often observed in both 14Cr and 9Cr ODS tube materials.
- Consistently with tensile tests, the tube creep test show no tertiary creep stage associated to a brutal cracking and leakage.

6. Acknowledgements

This work has been supported by the MatISSE European H2020 program. We kindly thanks Elodie ROUESNE (CEA) for SEM-EBSD characterisation of materials and Sébastien VINCENT for his contribution to creep matrix definition. The SAFIR2018 programme is acknowledged for development of the Crebello biaxial testing system at VTT. At EDF, Emmanuelle SCHOENER (EDF) for creep test performance, Martine BLAT (EDF) for material discussions and Frédéric DELABROUILLE (EDF) for microscopic investigations are acknowledged.

7. CRediT author statement

Denis Sornin: Resources, Writing-original draft, investigation

Ulla Ehrnstén: Supervision, Conceptualization, Resources, summarizing results

Juhani Rantala: Methodology, Investigation Data curation

Mario Walter: Resources, Investigations

Alexander Hobt: Investigation, Methodology

Lukas Frank: Investigation, Methodology

Andreas Ulbricht: Investigation; Writing – review and editing

Nathanael Mozzani: Resources, Methodology, Investigations

Solène Gicquel: Concept, Resources

Elvira Oñorbe: Investigation, Data Curation

Mercedes Hernández-Mayoral: Investigation, Data Curation, Writing-Original Draft

Yann de Carlan: Concept, supervision

The authors declare that they have no conflict of interest.

The raw/processed data required to reproduce these findings cannot be shared at this time as the data also forms part of an ongoing study

Annex: Tube creep matrix table for 9Cr ODS and 14Cr ODS steel

8. References

[1] B. Gwinner, M. Auroy, D. Mas, A. Saint-Jevin, S. Pasquier-Tilliette, Journal of Nuclear Materials, (2012), 428, 110-116.

[2] I. Proriol Serre, O. Hamdane, J.-B. Vogt, Nuclear Engineering and Design, (2017), 320, 17-27.

[3] P. Yvon, F. Carre, Journal of Nuclear Materials, (2009), 385, 217-222.

[4] T. Chen, E. Aydogan, J.G. Gigax, D. Chen, J. Wang, X. Wang, S. Ukai, F.A. Garner, L. Shao, Journal of Nuclear Materials, (2015), 467, 42-49.

[5] R.L. Klueh, Philosophical Magazine, (2018), 98:28 2618-2636.

[6] Y. de Carlan, J.-L. Bechade, P. Dubuisson, J.-L. Seran, Journal of Nuclear Materials, (2009), 386-388, 430-432.

[7] T. Kaito, Y. Yano, S. Ohtsuka, M. Inoue, K. Tanaka, A.E. Fedoseev , A.V. Povstyanko, A. Novoselov, Journal of Nuclear Science and Technology, (2013), 50:4, 387-399.

[8] G.R. Odette, Scripta Materialia, (2018), 143, 142-148.

[9] S. Ukai (Ed.) Microstructure and high temperature strength of 9Cr ODS ferritic steel., 2011.

[10] J. Malaplate, F. Mompiou, J.L. Béchade, T. Van Den Berghe, M. Ratti, Journal of Nuclear Materials, (2011), 417, 205-208.

[11] R.L. Klueh, P.J. Maziasz, I.S. Kim, L. Heatherly, D.T. Hoelzer, N. Hashimoto, E.A. Kenik, K. Miyahara, Journal of Nuclear Materials, (2002), 307-311, 773-777.

[12] H. Salmon-Legagneur, S. Vincent, J. Garnier, al., Material Sciences and Engineering, (2018), A722, 231-241.

[13] T. Tanno, Y. Yano, H. Oka, S. Ohtsuka, T. Uwaba, T. Kaito, Nuclear Materials and Energy, (2016), 9, 353-359.

[14] Y. Li, J. Zhang, Y. Shan, W. Yan, Q. Shi, K. Yang, J. Shen, T. Nagasasa, T. Muroga, H. Yang, S. Kano, H. Abe, Journal of Nuclear Materials, (2019), 517, 307-314.

[15] T. Jaumier, S. Vincent, L. Vincent, R. Desmorat, Journal of Nuclear Materials, (2019), 518, 274-286.

[16] D.L. Sornin, A. Karch, R.E. Logé, Journal of Materials Science, (2018), 53, 2965-2975.

[17] L. Toualbi, C. Cayron, P. Olier, R. Logé, Y. de Carlan, Journal of Nuclear Materials, (2013), 442, 410-416.

[18] T. Kaito, S. Ohtsuka, M. Inoue, T. Asayama, T. Uwaba, S. Mizuta, S. Ukai, T. Furukawa, C. Ito, E. Kagota, R. Kitamura, T. Aoyama, T. Inoue, Journal of Nuclear Materials, (2009), 386-388, 294-298.

[19] P. Dubuisson, Y. de Carlan, V. Garat, M. Blat, Journal of Nuclear Materials, (2012), 428, 6-12.

[20] O. Doyen, B.L. Gloannec, A. Deschamps, F.D. Geuser, C. Pouvreau, A. Poulon-Quintin, Journal of Nuclear Materials, (2019), 518, 326-333.

[21] G. Cao, NEUP report 10-925 (University of Wisconsin-Madison), (2013), 22.

[22] M.J. Bird, Monterey, California: Naval Postgraduate School. report 2014-6. http://hdl.handle.net/10945/42582 (2014), 91.

[23] M. Inoue, T. Kaito, S. Ohtsuka, Research and Development of Oxide Dispersion Strengthened Ferritic Steels for Sodium Cooled Fast Breeder Reactor Fuels, in: V. Ghetta, D. Gorse, D. Mazière, V. Pontikis (Eds.), Materials Issues for Generation IV Systems, Springer Netherlands, Dordrecht, 2008, pp. 311-325.
[24] S. Ukai, R. Miyata, S. Kasai, N. Oono, S. Hayashi, T. Azuma, R. Kayano, E. Maeda, S. Ohtsuka, Materials Letters, (2017), 209, 581-584.
[25] R. Pohja, Moilanen, P., Rantala, J., Huotilainen, S., Tulkki, V., Ehrnstén, U. & Holmström, S., 2016, In: Athens Journal of Sciences. , Athens Journal of Sciences, (2016), 3 227-240.
[26] C. Cayron, A. Montani, D. Venet, Y. De Carlan, Journal of Nuclear Materials, (2010), 399, 219-224.
[27] S. Ukai, R.J.M. Konings, 4.08 - Oxide Dispersion Strengthened Steels, Comprehensive Nuclear Materials, Elsevier, Oxford, 2012, pp. 241-271.
[28] T. Yamashiro, S. Ukai, N. Oono, S. Ohtsuka, T. Kaito, Journal of Nuclear Materials, (2016), 472, 247-251.
[29] N. Roduit, JMicroVision. https://jmicrovision.github.io/, 2020.
[30] E. Oñorbe, M. Hernández-Mayoral, A. Morrison, M. Serrano, Nuclear Materials and Energy, (2019), 20, 100698.
[31] "Online ILL data" https://doi.ill.fr/10.5291/ILL-DATA.1-01-146., 2015.
[32] J.-L. Lin, K. Mo, D. Yun, Y. Miao, X. Liu, H. Zhao, D.T. Hoelzer, J.-S. Park, J. Almer, G. Zhang, Z. Zhou, J.F. Stubbins, A.M. Yacout, Journal of Nuclear Materials, (2016), 471, 289-298.
[33] M.H. Mathon, M. Perrut, S.Y. Zhong, Y. de Carlan, Journal of Nuclear Materials, (2012), 428, 147-153.
[34] T. Tanno, S. Ohtsuka, Y. Yano, T. Kaito, Y. Oba, M. Ohnuma, S. Koyama, K. Tanaka, Journal of Nuclear Materials, (2013), 440, 568-574.